J. Fluid Mech. (2009), *vol.* 641, *pp.* 489–496.
doi:10.1017/S0022112009992138

Wake-mediated synchronization and drafting in coupled flags

SILAS ALBEN†

School of Mathematics, Georgia Institute of Technology, Atlanta, GA 30332-0160, USA

(Received 16 July 2009; revised 9 September 2009; accepted 10 September 2009; first published online 16 November 2009)

A recent experiment has shown 'inverted drafting' in flags: the drag force on one flag is increased by excitation from the wake of another. Here we use vortex sheet simulations to show that inverted drafting occurs when the flag wakes add coherently to form strong vortices. By contrast, normal drafting occurs for higher frequency oscillations, when the vortex wake becomes more complex and mixed on the scale of the flag. The types of drafting and dynamics (synchronization and erratic flapping) depend on the separation distance between the flags. For both tandem and side-by-side flags in synchronized flapping, the phase difference depends nearly monotonically on separation distance.

1. Introduction

Several recent experiments (Zhang *et al.* 2000; Watanabe *et al.* 2002; Epureanu, Tang & Païdoussis 2004; Shelley, Vandenberghe & Zhang 2005; Eloy *et al.* 2008), simulations and models (Theodorsen 1935; Zhu & Peskin 2002; Argentina & Mahadevan 2005; Alben 2008; Alben & Shelley 2008) have studied how a flag flaps in a flow. Flags present a canonical example of the 'flutter' instability observed in aircraft, bridges and other structures (Jain, Jones & Scanlan 1996; Bisplinghoff & Ashley 2002), and are thus a useful system for understanding fluid-structure interactions. The instability of a flag to flapping depends on the interplay of fluid pressure, flag inertia and bending forces. Bending rigidity tends to stabilize the flag. Lower flag density can also stabilize the flag, when the density is low enough (Argentina & Mahadevan 2005; Shelley *et al.* 2005; Alben 2008). Fluid pressure forces can be stabilizing or destabilizing depending on the physical parameters and the instantaneous flag configuration within a flapping cycle (Alben 2008).

Many interesting examples of locomotion in fluids involve active or passive elastic bodies interacting through their vortex wakes (Lissaman & Shollenberger 1970; Weimerskirch *et al.* 2001; Videler 1993; Drucker & Lauder 2001). The case of multiple flags allows for the interesting possibility of different forms of synchronization between the flags as a function of the distance between the flags. At different *transverse* distances, phase differences of approximately zero and π between the flapping flags were observed in experiment (Zhang *et al.* 2000) and simulation (Zhu & Peskin 2003; Farnell, David & Barton 2004; Tang & Païdoussis 2009). A linear stability analysis has shown some parameters for which the zero phase or π phase is the most unstable mode (Jia *et al.* 2007). There has been some mention of intermediate

† Email address for correspondence: alben@math.gatech.edu

flapping states for which the flags have phase between zero and π, as well as states which are unsynchronized. For the large-amplitude studies, the focus is mainly on the flag dynamics and less on the vortex wakes.

A messier but more dramatic interaction occurs for tandem flags, for which one flag lies directly behind another and thus experiences its wake more directly. For small separation distances the trailing flag is somewhat like a splitter plate, which can disrupt wake oscillation behind a static cylinder (Batchelor 1967). However, the oscillation of the upstream flag allows for an oscillatory flow. Ristroph & Zhang (2008) showed a drag reduction on the leading flag, and a drag increase on the follower, essentially the opposite of the steady drafting situation.

2. Two-flag model

Here we adapt the inviscid vortex sheet model used by Alben & Shelley (2008) and Alben (2009) to study the dynamics of two flags in the side-by-side and tandem configurations, and their vortex wakes. We consider two identical two-dimensional flags as inextensible elastic sheets of length L, mass per unit length ρ_s and rigidity B, moving under the pressure forces of a surrounding inviscid and incompressible fluid of density ρ_f (here, mass per unit area) that moves past the flag with free-stream speed U.

Scaling space on $L/2$, and time on L/U, the flag with complex position $\zeta(s,t)$ (s is arclength; $-1 \leqslant s \leqslant 1$) evolves via Newton's second law as

$$R_1 \partial_{tt}\zeta = \partial_s(T\hat{\mathbf{s}}) - R_2\partial_s(\partial_s\kappa\hat{\mathbf{n}}) - [p]\hat{\mathbf{n}}, \tag{2.1}$$

where T is the tension that enforces inextensibility, $[p]$ is the pressure jump across the flag and κ is the flag curvature. The tension has been scaled by $\rho_f U^2 L/2$, the pressure by $\rho_f U^2$, and R_1 and R_2 are the two control parameters of the dynamical system with $R_1 = 2\rho_s/\rho_f L$ the dimensionless mass of the flag and $R_2 = 8B/\rho_f U^2 L^3$ its dimensionless rigidity (also an inverse square velocity). The sheet is held and clamped at $s = -1$, its leading end, with zero deflection. Free-end boundary conditions are assumed at $s = 1$ with $T = \kappa = \kappa_s = 0$ there, and the tension can be eliminated from (2.1) by integration of the $\hat{\mathbf{s}}$ component from $s = 1$.

The flow is inviscid and irrotational outside of a bound vortex sheet on each flag, and free vortex sheets which emanate from the trailing edges of each flag. The fluid velocity is a sum of a horizontal background flow with speed unity and the flow induced by the vortex sheets:

$$\mathbf{u}(\mathbf{x}) = \hat{\mathbf{e}}_{\mathbf{x}} + \frac{1}{2\pi i}\int_C \frac{\gamma(s',t)\,\mathrm{d}s'}{\zeta(s,t)-\zeta(s',t)}. \tag{2.2}$$

The bound vortex sheet strength γ is determined by the condition that fluid velocity and flag velocity v normal to each flag are equal:

$$v(s,t) = \hat{n}\cdot\hat{\mathbf{e}}_{\mathbf{x}} + \hat{n}\cdot\frac{1}{2\pi i}\int_C \frac{\gamma(s',t)\,\mathrm{d}s'}{\zeta(s,t)-\zeta(s',t)}. \tag{2.3}$$

Solving (2.3) requires an additional constraint on the total circulation about each flag and its shed vortex sheet. For a flow started from rest the total circulations are zero. At each instant the part of the circulation in the free sheet, or equivalently, the strength of γ where the free sheet meets the trailing edge of the body, is set by the Kutta condition which makes velocity finite at the trailing edge. At every other point of the free sheet, γ is set by the criterion that circulation (the integral of γ) is

conserved at material points of the free sheet. Material points of the free sheet are advected by the fluid velocity in (2.2). The pressure is determined in terms of γ by a version of the unsteady Bernoulli equation

$$\partial_t \gamma + \partial_s((\mu - \tau)\gamma) = \partial_s[p], \tag{2.4}$$

where μ is the average flow velocity tangent to the body, and τ the tangential body velocity. At the trailing edge, $[p] = 0$.

We neglect shear stresses and gravity, which can provide a stabilizing tension in the flag (Argentina & Mahadevan 2005; Shelley *et al.* 2005; Eloy *et al.* 2008), and three-dimensional effects, which are considered by Eloy *et al.* (2008).

We numerically solve the nonlinear system of equations (2.1), (2.3) and (2.4), and boundary conditions at each time step using a Broyden solver (Ralston & Rabinowitz 2001). The free vortex sheet is moved with an explicit scheme for ordinary differential equations, second order in the time step. The spatial and temporal discretization and convergence studies for the model with a single body are given in Alben (2009). On the free sheet, the singular kernel $1/(\zeta - \zeta')$ is mollified and replaced by the smoothed kernel $\overline{\zeta - \zeta'}/(|\zeta - \zeta'|^2 + \delta^2)$ to suppress the growth of numerical instabilities, as used by Krasny (1986) and many others since. Here we use $\delta = 0.2$; information on convergence as $\delta \to 0$ is given by Krasny (1986) and Alben (2009).

3. Side-by-side flapping

In Alben & Shelley (2008) we found a stability boundary for the flag in R_1–R_2 space, and moving into the region of instability, a series of transitions from flapping with a single period to 'chaotic' flapping with a broad spectrum of frequencies. We now focus on coupled flapping behaviours at the values $R_1 = 0.6$, $R_2 = 0.014$, which give periodic flapping for a single flag. These behaviours may also be relevant to future work on periodically driven elastic bodies. Essentially the same behaviour is found at other R_1–R_2 values which yield periodic flapping.

We first consider two flags flapping side-by-side, with their leading edges separated by a distance d_y (figure 1). We ramp up the background flow smoothly to unity for $0 < t < 0.2$, and smoothly apply a small perturbation (a vertical displacement of $O(10^{-2})$ at the leading edge) to the upper flag. No perturbation is applied to the lower flag, and both flags are clamped at fixed d_y after $t = 0.2$. We track the dynamics over many (70–100) flapping periods.

In figure 1(*a*) we show a snapshot characteristic of the irregular flapping behaviour for $d_y = 1$ (and all $d_y \lesssim 1.8$). In figure 1(*d*) we plot the vertical position of the flags' ends versus time for $d_y = 1$. At different time intervals in this single simulation, the flags may flap: nearly in phase ($5 < t < 25$, $110 < t < 115$, $195 < t < 200$); more often, nearly out of phase ($35 < t < 50$, $60 < t < 90$, $120 < t < 140$, $150 < t < 185$); with one flag having much larger amplitude than the other (near $t = 30, 55, 95$); or irregularly. The dynamics switch abruptly between these behaviours. In figure 1(*a*) the physical reason is shown: the trailing edges of the flags nearly collide. In such close approaches the subsequent flapping behaviour is highly sensitive to small perturbations. For smaller d_y the flags may collide, but we do not present data from such simulations in this work. In figure 1(*b*), d_y is increased to 1.8, and opposite-phase flapping is now the only attracting state. We plot the average phase between the flags in figure 1(*e*) (solid line with crosses). The average phase is defined as the average temporal displacement between maxima in end deflections for the lower flag and the upper flag, divided by the average displacement between maximum deflections for the upper flag (the

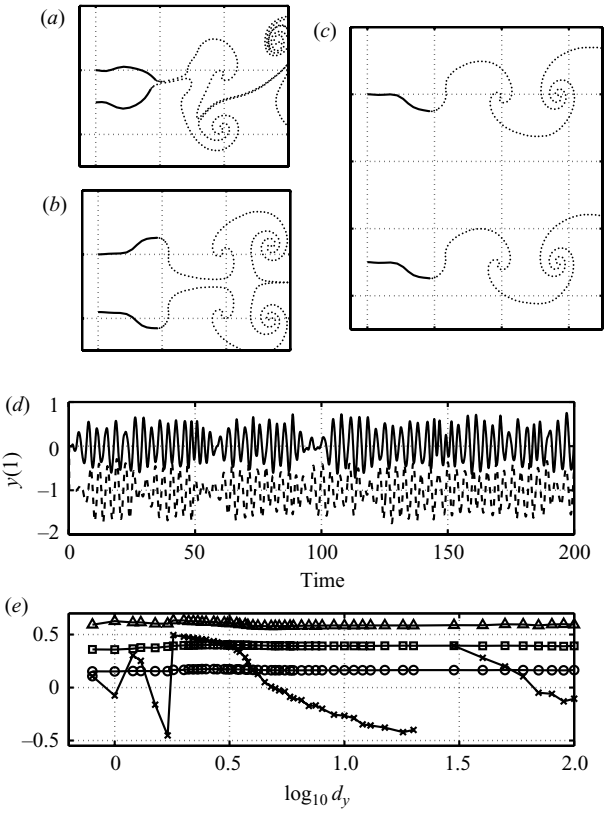

FIGURE 1. (*a–c*) Snapshots of flags (solid lines) and wakes (dotted lines) for $d_y = 1$ (*a*), 1.8 (*b*), 5 (*c*). In all cases $R_1 = 0.6$, $R_2 = 0.014$. (*d*) For $d_y = 1$, the vertical positions of ends of the top flag (solid) and bottom flag (dashed) versus time. (*e*) The three nearly horizontal lines are: root mean square (RMS) vertical force $\sqrt{\langle F_y^2 \rangle}$ (triangles), RMS end deflection $\sqrt{\langle y(1)^2 \rangle}$ (squares) and time-averaged horizontal force $\langle F_x \rangle$ (circles). The fourth line (crosses) shows the phase difference between the flags in units of a flapping period.

average period). The average phase is erratic for $d_y < 1.8$, reflecting the lack of simple periodic flapping for very close flags. At $d_y = 1.8$, the flags have opposite phase (the value 0.5), which then changes somewhat smoothly to flapping in phase when $d_y = 5$ (snapshot in figure 1*c*). The phase changes nearly monotonically with d_y up to $d_y = 10^2$. In figure 1(*e*) we also plot the root mean square (RMS) vertical force (triangles), RMS end deflection (squares) and average horizontal force (circles). All have small variations for d_y down to 0.6, showing that even for fairly small side-by-side displacements the average forces on each flag are not strongly affected by the other.

4. Tandem flags

We now set d_y to zero and set the leading edge of one flag (the follower) a distance d_x behind the trailing edge of the other (the leader). In figure 2(*a–e*) we give snapshots at five increasing values of d_x. In figure 2(*a*, *c*, *e*) the follower is nearly synchronized with (though phase shifted from) the leader, and the flags' wakes combine to form coherent vortices and dipoles behind the follower, resulting in a large force on the

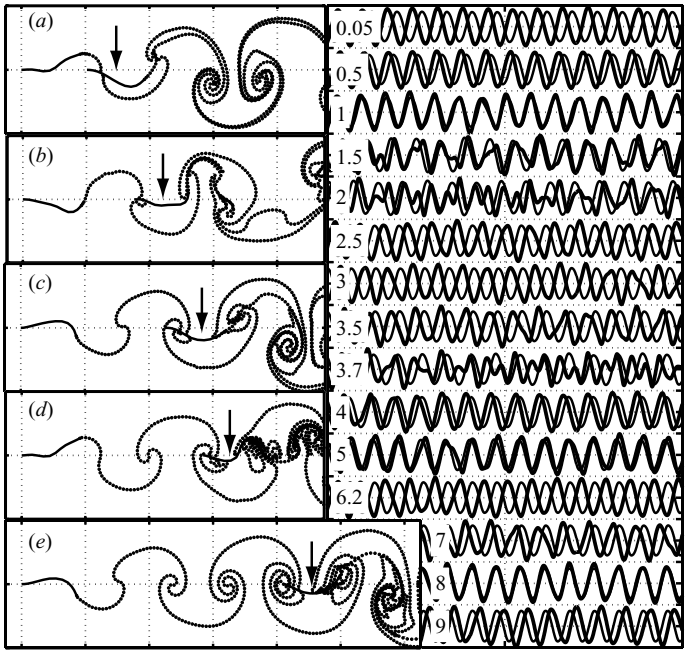

FIGURE 2. Snapshots of flags (solid lines) and wakes (dotted lines) for $d_x = 0.05$ (*a*), 1.5 (*b*), 2.5 (*c*), 3.7 (*d*) and 6.2 (*e*). Arrows indicate the midpoint of the trailing flag. In all cases $R_1 = 0.6$, $R_2 = 0.014$. Right panel: Vertical positions of the ends of the leader flag (solid) and follower flag (heavier dashed line) for $125 < t < 175$ and various d_x (listed at left).

follower. A similar constructive interaction occurs between the dorsal fin wake and the caudal fin in Bluegill sunfish (Drucker & Lauder 2001). In the intermediate cases (figures 2*b* and 2*d*), the follower flaps erratically, the wakes do not combine coherently, and the force on the follower is reduced.

The right panel of figure 2 shows end deflections for the two flags (follower in bold) for figure 2(*a–e*) and many other values of d_x. For $0.05 < d_x < 1$ the flags are nearly synchronized with phase varying smoothly with d_x. At $d_x = 1.5$ and 2 the follower flaps erratically, and synchronization begins again at $d_x = 2.5$. Erratic flapping occurs again at $d_x = 3.7$.

The effect of synchrony or erratic flapping on the flags forces and dynamics is shown in figure 3. We find that the average period of the follower drops when flapping becomes erratic, though the size of such drops decreases at larger d_x (figure 3*a*, circles), for which the wake is wider when it impinges on the follower. In figure 3(*b*), the average phase difference between leader and follower decreases smoothly and with nearly constant slope as d_x increases, somewhat akin to figure 1(*e*) but now the horizontal scale is linear. In figure 3(*c*) we find that the RMS deflection of the follower (circles) is often significantly larger than that of the leader (crosses), but drops when flapping becomes erratic. Similarly, the horizontal force on the follower is greater than that of the leader when flapping is synchronous, and also drops when flapping becomes erratic (figure 3*d*, circles). This 'inverted drafting' is qualitatively quite similar to the experimental results in figure 2 of Ristroph & Zhang (2008), though there the follower curve drops more smoothly as d_x increases, and the relationship between inverted drafting, synchrony and coherence of vortex wakes is new here. We also find that the drag on the leader drops to about 70 % of that on a lone flag as the

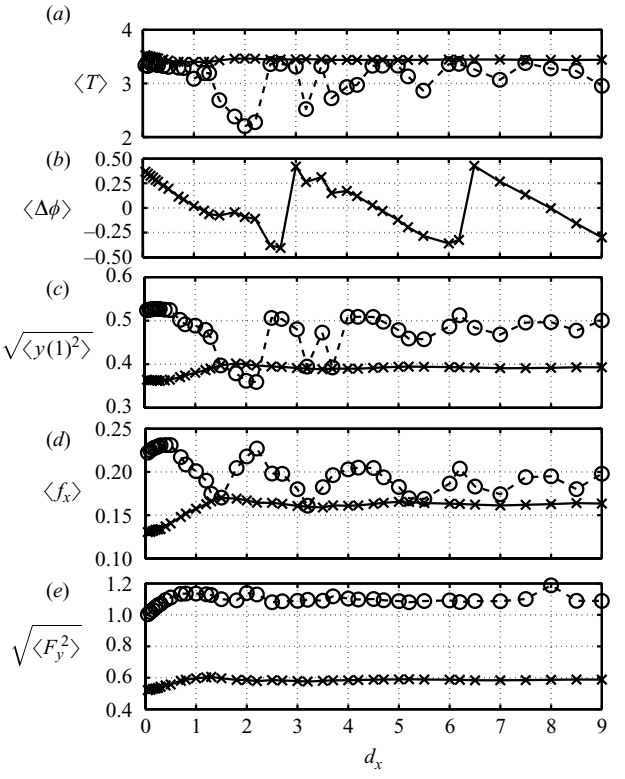

FIGURE 3. For the leader flag (solid line, crosses) and follower flag (dashed line, circles), time averaged period (a), phase difference between the flags (b), end amplitude (c), horizontal force (d) and RMS vertical force (e) versus d_x. In all cases $R_1 = 0.6$, $R_2 = 0.014$.

separation between the flags decreases from a half-length down to zero. Ristroph & Zhang (2008) also found that the leader drag decreases over this separation range, by a somewhat larger amount (down to about 55 % of the lone-flag drag). The lone-flag drag is 0.164, the same as the leader drag for large d_x (but not the follower flag, which is influenced by the (undiffused) leader wake even at large d_x). The RMS vertical forces, shown in figure 3(e), are much steadier with d_x, and again much greater for the follower.

The d_x for synchronized flapping are given by the peaks in follower drag in figure 3(d), and are spaced by approximately 2. This is nearly the spacing between positive and negative vortices in the vortex streets of figure 2. If the flags' wakes synchronize at any one d_x, we expect they will also synchronize when the follower moves downstream by a vortex-spacing, and flaps with opposite phase (to match the oppositely-signed vortices that it now encounters). At the intermediate values of d_x, the flags' wakes add destructively and erratic flapping occurs.

We now consider results with the flags' rigidities R_2 decreased from 0.014 to 0.011. An isolated flag would flap with higher frequency and bending mode, indicated by the compressed vortex wake of the leader in figure 4(a) compared with the leader wake in figure 2(c) (and see Alben & Shelley 2008). The vortex sheet is now much more complex as it impinges on the follower in figure 4(a), and the follower now flaps erratically for all d_x at this lower R_2. Figure 4(b) shows a striking reversal from figure 3(d, e) in the relative forces: the follower experiences horizontal drag

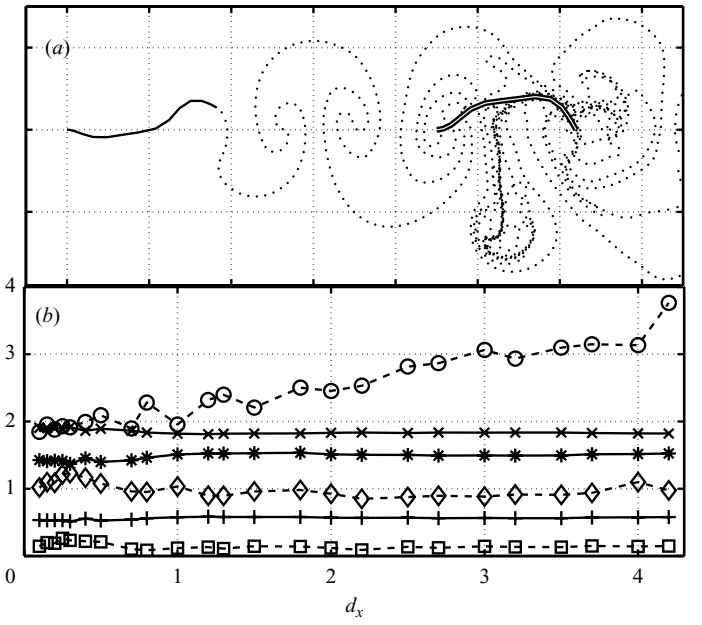

FIGURE 4. (*a*) Snapshot of flags (leader: solid line; follower: outlined line) for $R_1 = 0.6$, $R_2 = 0.011$, and $d_x = 2.5$. (*b*) Time-averaged quantities versus d_x: period between successive maxima of end deflection (leader: crosses, follower: circles); RMS vertical force (leader: asterisks, follower: diamonds); horizontal force (leader: plusses, follower: squares).

much lower than (one-third to one-half) that of the leader and one-half to two-thirds the RMS vertical force. The reason is that the wake of the leader is wider and more rolled-up, and its positive and negative vorticity are more mixed when they encounter the follower. Consequently the follower encounters a slower oncoming flow velocity, similar to that in steady drafting, and unlike the more coherent periodic wakes in figure 2. The peaks in follower forces in figure 4(*b*) are more closely spaced, corresponding to the closer spacing between vortices in the leader wake in figure 4(*a*).

Our simulations have shown how synchrony and erratic flapping arise in side-by-side and tandem flags. These results may be used to search for optimal rigidities and separation distances for bodies in collective locomotion. Future work will address: nonidentical flags, for which an unstable flag may provide external forcing to a stable flag; and flags separated by non-zero d_x and d_y, which might be classified based on whether the leader's wake passes along one or both sides of the follower.

We acknowledge support from NSF-DMS Grant 0810602.

REFERENCES

ALBEN, S. 2008 The flapping-flag instability as a nonlinear eigenvalue problem. *Phys. Fluids* **20**, 104106.

ALBEN, S. 2009 Simulating the dynamics of flexible bodies and vortex sheets. *J. Comput. Phys.* **228** (7), 2587–2603.

ALBEN, S. & SHELLEY, M. J. 2008 Flapping states of a flag in an inviscid fluid: bistability and the transition to chaos. *Phys. Rev. Lett.* **100**, 074301.

ARGENTINA, M. & MAHADEVAN, L. 2005 Fluid-flow-induced flutter of a flag. *Proc. Natl Acad. Sci. USA* **102**, 1829–1834.

Batchelor, G. K. 1967 *An Introduction to Fluid Dynamics*. Cambridge University Press.

Bisplinghoff, R. L. & Ashley, H. 2002 *Principles of Aeroelasticity*. Dover.

Drucker, E. G. & Lauder, G. V. 2001 Locomotor function of the dorsal fin in teleost fishes: experimental analysis of wake forces in sunfish. *J. Exp. Biol.* **204** (17), 2943–2958.

Eloy, C., Lagrange, R., Souilliez, C. & Schouveiler, L. 2008 Aeroelastic instability of a flexible plate in a uniform flow. *J. Fluid Mech* **611**, 97–106.

Epureanu, B. I., Tang, L. S. & Paidoussis, M. P. 2004 Coherent structures and their influence on the dynamics of aeroelastic panels. *Intl J. Non-Linear Mech.* **39** (6), 977–991.

Farnell, D. J. J., David, T. & Barton, D. C. 2004 Coupled states of flapping flags. *J. Fluid. Struct.* **19** (1), 29–36.

Jain, A., Jones, N. P. & Scanlan, R. H. 1996 Coupled flutter and buffeting analysis of long-span bridges. *J. Struct. Engng* **122** (7), 716–725.

Jia, L. A. I. B., Li, F., Yin, X. I. E. Z. & Yin, X. I. E. Y. 2007 Coupling modes between two flapping filaments. *J. Fluid Mech.* **581**, 199–220.

Krasny, R. 1986 Desingularization of periodic vortex sheet roll-up. *J. Comput. Phys.* **65**, 292–313.

Lissaman, P. B. S. & Shollenberger, C. A. 1970 Formation flight of birds. *Science* **168** (3934), 1003.

Ralston, A. & Rabinowitz, P. 2001 *A First Course in Numerical Analysis*. Dover.

Ristroph, L. & Zhang, J. 2008 Anomalous hydrodynamic drafting of interacting flapping flags. *Phys. Rev. Lett.* **101**, 19.

Shelley, M., Vandenberghe, N. & Zhang, J. 2005 Heavy flags undergo spontaneous oscillations in flowing water. *Phys. Rev. Lett* **94**, 094302.

Tang, L. & Païdoussis, M. P. 2009 The coupled dynamics of two cantilevered flexible plates in axial flow. *J. Sound Vib.* **323**, 790–801.

Theodorsen, T. 1935 General theory of aerodynamic theory and the mechanism of flutter. *Tech. Rep.* 496. NACA.

Videler, J. J. 1993 *Fish Swimming*. Springer.

Watanabe, Y., Suzuki, S., Sugihara, M. & Sueoka, Y. 2002 An experimental study of paper flutter. *J. Fluids Struct.* **16** (4), 529–542.

Weimerskirch, H., Martin, J., Clerquin, Y., Alexandre, P. & Jiraskova, S. 2001 Energy saving in flight formation. *Nature* **413** (6857), 697–698.

Zhang, J., Childress, S., Libchaber, A. & Shelley, M. 2000 Flexible filaments in a flowing soap film as a model for one-dimensional flags in a two-dimensional wind. *Nature* **408** (6814), 835–839.

Zhu, L. & Peskin, C. S. 2002 Simulation of a flapping flexible filament in a flowing soap film by the immersed boundary method. *J. Comput. Phys.* **179**, 452–468.

Zhu, L. & Peskin, C. S. 2003 Interaction of two flapping filaments in a flowing soap film. *Phys. Fluids* **15**, 1954–1960.